Influence of Environmental Conditions on Caking Mechanisms in Individual Amorphous Food Particle Contacts

Christine I. Haider, Michael J. Hounslow, and Agba D. Salman
Dept. of Chemical and Biological Engineering, University of Sheffield, Mappin Street, Sheffield S1 3JD, U.K.

Tim O. Althaus
Dept. of Science, Nestlé Product Technology Centre, Haxby Road, York YO31 8FZ, U.K.

Gerhard Niederreiter and Stefan Palzer
Dept. of Research and Development, Nestlé SA Headquarters, Avenue Nestlé 55, CH-1800 Vevey, Switzerland

Caking of amorphous powders creates severe problems such as product loss and additional costs in the food industry. Among the main factors causing this unwanted agglomeration process are fluctuations of the environmental conditions, that is, a rise in temperature and humidity. There is correspondingly a need to identify and, if possible, avoid the environmental conditions inducing strong interparticle cohesion based on particle contact mechanisms like viscoelastic flattening and sintering. For this reason, a novel micromanipulation approach focusing on the interactions between individual amorphous food particles in contact under load in a controlled environment is introduced. It was possible to identify the dominant caking mechanism under defined conditions, such as temperature and humidity, particle deformation, as well as contact holding time, and to quantify interparticle cohesion. Furthermore, the mechanical behavior of rubbery spherical model particles is presented and a theoretical approach to describe the contact zone formation kinetics is proposed. © 2014 American Institute of Chemical Engineers *AIChE J*, 60: 2774–2787, 2014
Keywords: particle technology, food, rheology, materials, mechanics

Introduction

Powder processing is of great importance in numerous industries such as the food, chemical, and pharmaceutical industries. Especially in the food industry, many products are dehydrated or dried to obtain powders that can be reconstituted with the advantages of, for example, the reduction of their transport weight and the improvement of their shelf life due to decreased susceptibility to microorganisms.[1] Examples are maltodextrins, granulated sugar, spray-dried dairy powders, powdered vegetable, yeast and meat extracts, flavor powders as well as freeze-dried juice concentrate.[2–4] Many of these examples consist of or at least contain a considerable amount of amorphous water-soluble material. An amorphous supra-molecular glassy powder structure can be formed on rapid dehydration and/or cooling of liquids as is the case in spray drying, which is a widely used unit operation in the food industry.[4,5]

These powders containing amorphous water-soluble substances or being entirely composed of them are particularly prone to adhering to equipment due to stickiness and caking, which is the most common unwanted agglomeration mechanism of food bulk material. It causes various issues for both the powder manufacturing industry as well as consumer per-

ception.[2,4,6] In particular during processing in a factory, caking can lead to the contamination of equipment and time consolidation during storage in silos. This results in product loss and makes additional production steps like delumping, milling, and grinding operations on powder cakes or the addition of anti-caking agents and the corresponding extra costs necessary.[2,7,8] Furthermore, consumer satisfaction is negatively influenced by lumps in powdered end products and posthardening of amorphous tablets compromising their rehydration capacity, ease of handling and even general quality concerning aroma, shelf life, and nutrients.[4,9,10]

Accordingly, it is of great importance for the food industry to avoid caking of amorphous powders and the negative effects connected to it. This can be achieved by circumventing process conditions that trigger unwanted agglomeration based on stickiness and viscous flow of material between particles. It has been found that the environmental conditions, temperature, and humidity, are thereby the key external factors in addition to compressive stress.[2,4,6,11,12]

The environmental conditions expressed in the quantity $T - T_g$, which is defined as the difference between the temperature of the environment T and the onset glass transition temperature of the material T_g, are directly linked to the caking rate or kinetics and the caking mechanism.[2,8] No caking can be observed on a relevant time scale in free flowing glassy powders with a negative $T - T_g$.[4] In the rubbery state or glass transition regime, depending on the actual positive difference between T and T_g, the interparticle cohesion and

Correspondence concerning this article should be addressed to A. D. Salman at a.d.salman@sheffield.ac.uk.

caking probability can be increased due to enhanced particle deformability, viscoelastic, and/or plastic flattening in conjunction with van der Waals interactions or sticking of the particles and sintering.[2,5,9] Sintering describes the bridge formation between two neighboring particles and their potential fusion due to the flow of molecules into the contact zone.[5]

The difference $T - T_g$ can easily be increased to positive values in a hot, humid environment where T is elevated and T_g decreases for hygrosensitive powders. The latter are most common in dehydrated food products and are characterized by the reduction of their T_g with increasing water content of the powder.[13] This is very critical for food powder processing in countries with a hot and humid climate as well as the transport of finished products containing amorphous material into these countries.[5] Moreover, temperature and humidity fluctuations based on differences between day and night, or a change in the seasons and weather including enhanced precipitation in a more moderate climate can be held responsible for caking during storage, further enhanced by the weight pressure of the powder bulk or capillary condensation between particle surfaces.[2,3,11,12] Additionally, production processes involving unit operations like spray-drying and fluid-bed agglomeration are at risk of being interrupted when critical temperature and humidity conditions are reached.[2]

Most previous investigations into caking are based on observations made in bulk studies and define if unwanted agglomeration occurs under a fixed set of conditions or not. In many cases, only comparative data are collected in extensive set of tests involving shear or uniaxial experiments on bulk solids stored under divergent environmental conditions. This requires large amounts of powder that might not be available in the early development of a new product.[7] In addition, equilibration processes within the environment prior to a test might be inhomogeneous and take a long time due to the large sample size.[14] Limited information is gained about the types of caking mechanisms occurring and how their kinetics can be described and, thus, controlled. This is because the development of interparticle contacts with time cannot be studied directly. The divergence of approaches and results emphasizes the lack of a standardized meaningful method for characterizing caking, which also becomes apparent in the literature.[4,8,15]

As caking and stickiness are related to the deformability and physical state of the surfaces of initially individual particles inside a bulk powder, there is an obvious need to directly investigate the formation of a contact zone and interactions between them. This work applies a new approach utilizing amorphous particle pair studies to identify the dominant caking mechanism, estimate the induced contact zone and quantify the resulting interparticle cohesion under defined contact times and deformation inside a controlled environment. The findings on particle pair level can be used for an estimation of the strength of the whole powder cake as well as for computer-assisted modeling of caking kinetics.

For all the aforementioned reasons, a novel device called a micromanipulation particle tester (MPT) has been used for interparticle studies on an amorphous hygrosensitive model material, maltodextrin dextrose equivalent (DE) 21, which is used in many powder formulations in the food industry. With the aid of this device, distance-controlled particle contact experiments can be performed whereby two particles are brought into contact and deformed. The evolving contact or sinter bridge diameter and possible changes in the particle shape are measured optically with a digital microscope.

Simultaneously, a load cell records the induced compressive force relaxation over a defined contact holding time and the resulting cohesion on separation between the tested particles. It is also equipped with an environmental chamber making it possible to manipulate the temperature and relative humidity of the test environment to adjust the critical parameter $T - T_g$. Based on the findings obtained with the MPT, the threshold conditions for which a transition from mere viscoelastic flattening and stickiness to sintering occurs can now be defined as well as the connected critical cohesion forces that are necessary for the formation of a stable powder cake.

A study applying short contact holding times of 3 s on amorphous maltodextrin DE 21 model food particles at a fixed deformation of 10% with varying $T - T_g$ values has been conducted to investigate the effect of the environmental conditions on the type of contact zone mechanism and resulting cohesion. Due to the short holding times tested, the results account mainly for the risk of instantaneous stickiness. If stickiness occurs during the residence time of powder in industrial equipment, it will cause severe problems to the whole manufacturing process. Moreover, an existing theoretical model has been adapted and tested against experimental results for the time-dependent contact zone formation. Additional experiments based on the application of longer contact times under defined temperature and humidity ramps showed the effects of temperature and humidity fluctuations on interparticle cohesion during storage.

Theoretical Background

In general, $T - T_g$ is an important measure for the caking probability and determines which caking mechanism can act on a defined time scale. This is due to its influence on the rheological behavior of an amorphous hygrosensitive material, which determines the flattening and sintering kinetics as well as the transition between these two different caking mechanisms. With increasing $T - T_g$, especially in the glass transition regime above T_g, the void spaces or free volume between the randomly distributed molecules in an amorphous matrix increase and enable enhanced molecular mobility.[1,16] With increasing positive values of $T - T_g$, the material viscosity drops several magnitudes from 10^{11-12} Pa.s to approximately 10^{6-8} Pa.s.[4,8,13,17,18] This relationship between $T - T_g$ and the viscosity can be described theoretically with the aid of the Williams, Landel, and Ferry (WLF) equation, which is valid for positive differences of $T - T_g$ up to 100°C and commonly utilized for food powders with an approximately constant density[19]

$$\log \frac{\eta}{\eta_g} = \frac{-C \cdot (T - T_g)}{B + (T - T_g)} \qquad (1)$$

The reference temperature used in the equation is the glass transition onset temperature of the material T_g. η and η_g are the viscosity at a certain temperature of the environment T and the viscosity of the amorphous substance in the glassy state or close to T_g (which is assumed to be 10^{12} Pa.s for maltodextrin DE 21 corresponding to a standard value from the literature for polymers),[16,20–22] respectively. The two constant factors C and B have the values 17.44 and 51.6 K and are applicable to the majority of polymers, which WLF investigated in their work.[19]

The quantity $T - T_g$ and, thus, the viscosity of an amorphous material can be changed by varying the temperature

of the environment T or by influencing T_g. The physicochemical properties of water-soluble amorphous matrices like their T_g can be altered by varying their moisture content. This is called hygrosensitive behavior.[1,16,22,23] The amorphous substance takes up or releases moisture in the air until it reaches equilibrium with the ambient relative humidity. In other words, until its water activity is similar to the relative humidity of the air. In addition, capillary condensation can occur and also lead to plastification. The water activity a_W of a substance is defined for a certain temperature by the ratio of the equilibrium vapor pressure above the system and the vapor pressure of pure water and gives an indication of the free water available on the surface and inside a substance.[21,24] If a true equilibrium with the environmental relative humidity is reached, a_W can be related to the water content on dry basis m (= amount of water divided by the mass of the dry substance) of an amorphous material via temperature-dependent sorption isotherms. To establish these, the Brunauer–Emmet–Teller model (BET) is frequently applied for food materials[25–29]

$$\frac{m}{m_m} = \frac{n \cdot a_W}{(1-a_W) \cdot (1+(n-1) \cdot a_W)} \quad (2)$$

whereby n is a fitting constant and m_m is referred to as the monolayer value equalling the number of water molecules in a monolayer on the surface of a material.[1,21,30]

Brunauer et al.[26] originally described sorption isotherms related to van der Waals adsorption of nonpolar gases on different nonporous solids. Although, for food materials, mostly polar gases and adsorbents, that is, water vapor, are of interest, a high applicability of the BET model to water sorption was found empirically, and the corresponding isotherms are widely used to determine the monolayer moisture content for foods.[31,32] The BET model can be extended with an additional parameter for a wider applicability to high a_W values accounting for multilayer adsorption.[33]

To derive the T_g based on the water content of the material, the Gordon and Taylor equation can be utilized for most amorphous soluble food products.[28] Therefore, the water content on dry basis m has to be transformed into the water content on wet basis w (= amount of water divided by the mass of the entire substance including contained water) and the fitting parameter k, which is also called Gordon and Taylor constant, has to be introduced. In addition, the glass transition onset temperatures of the pure substance, T_{gs}, and water, T_{gw} (= −135°C), have to be known[1,34,35]

$$T_g(w) = \frac{(1-w) \cdot T_{gs} + w \cdot k \cdot T_{gw}}{(1-w) + w \cdot k} \quad (3)$$

Caking occurs when a change in $T - T_g$ and the applied pressure on a powder enhance the cohesion between the contained individual particles and also the adhesion between a particle and, for example, the wall of a processing equipment. This rise in cohesion and adhesion, respectively, can be brought about by different caking or particle contact mechanisms. At the onset of the rubbery state of amorphous powders, that is, for low-positive values for $T - T_g$, viscoelastic flattening of particles in contact is one of the most important contact mechanisms. This creates larger contact zones between the particles and, thus, promotes attractive van der Waals forces.[4,22] The latter refer to finite ranged interactions based on temporary electrostatic load shifts of molecules on a particle surface. They act against repulsive
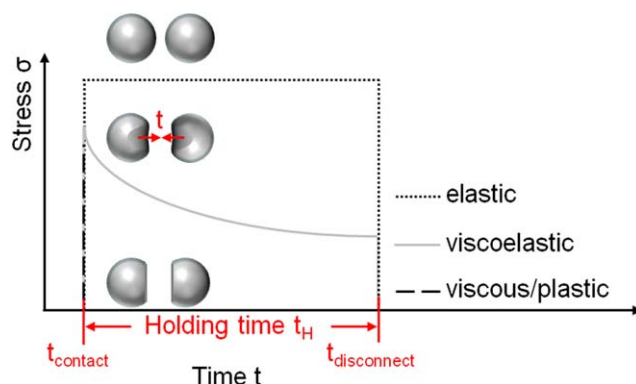

Figure 1. Schematic stress relaxation curves and deformation patterns for pairs of elastic, viscoelastic, and viscous/plastic particles during a defined holding time t_H for an instantaneous strain application at $t_{contact}$ and particle disconnection at $t_{disconnect}$.

[Color figure can be viewed in the online issue, which is available at wileyonlinelibrary.com.]

elastic energies which occur when viscoelastic particles are deformed.[36] Their influence is dependent on the size of the particles and the distance between them.[37] For surface separations smaller than 100 nm, these finite ranged interactions can even be strong enough to induce particle deformation. They are proportional to the inverse of the distance d squared between the particles and the resulting cohesion force can be calculated for two undeformed spheres according to the following expression[38]

$$F_H = \frac{A_H}{12} \cdot \frac{1}{d^2} \cdot \left(\frac{1}{a_1} + \frac{1}{a_2}\right)^{-1} \quad (4)$$

For particles with identical diameters $a = a_1 = a_2$, the sum in the brackets can be written as $2/a$. A_H is the Hamaker constant and is dependent on the material. In practice, a remaining distance of $d = z_0 = 0.4–0.5$ nm is commonly assumed for touching particles. The value z_0 corresponds to a minimum of the potential between the repulsion of the molecules and the van der Waals attraction.[38,39] Electrostatic forces other than van der Waals interactions also lead to cohesion between particles but can be considered negligible for food powders due to their small magnitude.[1]

While ideal elastic deformation of particles in contact under load is completely reversible and the application of larger external forces does not lead to cohesion force enhancement on separation, perfect plastic deformation is irreversible and facilitates additional van der Waals attraction in the flattened section.[40] Viscoelastic deformation lies between these two ideal cases. A viscoelastic material shows time-dependent deformation on load application and its mechanical properties are often investigated by transient relaxation tests (Figure 1). A relaxation test comprises the instantaneous application of a defined strain, which is then kept constant for a certain holding time while the degradation of the stress inside the material is recorded.[17] By fitting the obtained curve with an appropriate differential equation such as, for example, a simple two-parameter Maxwell or Kelvin–Voigt model, viscoelastic parameters describing the rheological behavior of the material can be obtained. In

many cases, however, a more complex mechanical model comprising three or more parameters is necessary to account accurately for experimental data and to define rheological parameters that are characteristic for an amorphous substance at a defined $T - T_g$.[41]

For materials with a so-called "delayed elasticity," that is, relaxation to a non-zero stress state, a three parameter mechanical model was described by Johnson,[42] which can be represented by a spring in series with a spring and a dashpot set in parallel. The corresponding differential equation for a relaxation test can be written as follows using the mechanical parameters E_1, E_2 and η_D[42]

$$\sigma(t) = \frac{E_1}{E_1 + E_2} \cdot \left(E_2 + E_1 \cdot e^{-\frac{t \cdot (E_1 + E_2)}{\eta_D}} \right) \cdot \varepsilon_0 \qquad (5)$$

It can also account for a complete relaxation of a material to a zero stress state. In this case, it reduces to the simple Maxwell model for $E_2 = 0$, which is the elasticity parameter that describes the spring set in parallel with the dashpot.

If, instead of a step increase in strain, an instantaneous stress is applied to such a material, its creep behavior can be observed, that is, the time-dependent deformation or experienced strain of the viscoelastic substance under load. Again, a differential equation using the same parameter set as the relationship for the relaxation of the material can be established[42]

$$\sigma(t) = \varepsilon_0 \cdot \frac{E_1}{E_1 + E_2} \cdot \left(E_2 \cdot e^{\frac{-t \cdot (E_1 + E_2)}{\eta}} \right) \qquad (6)$$

These parameters can also be used in calculations describing, for instance, the time-dependent development of the contact zone between two viscoelastic spheres fixed in a constant position under load.

One example of such a modeling approach is based on Wei Hsuin.[43] This author derived an expression for the growth kinetics of the contact zone of linear viscoelastic and isotropic bodies with an arbitrary quadratic surface profile under load. Therefore, Wei Hsuin generalized the classic Hertz contact theory to also include the description of the contact of viscoelastic bodies under the prerequisite of a monotonically increasing indentation. Further assumptions are the exclusion of friction, small strains and large measures of the viscoelastic bodies in comparison to the contact zone size. For two spheres of the same homogeneous, isotropic and linearly viscoelastic material, the contact diameter x can be described with the following relationship for a preserved spherical shape of the particles[40,43]

$$\left(\frac{x}{a} \right)^3 \approx 3 \cdot \frac{F_t}{a^2} \cdot k(t) \qquad (7)$$

where $k(t)$ is a characteristic material function in the linear viscoelastic regime. F_t is the total force the particles are pressed together with including van der Waals attraction, t is the contact time and a is the particle diameter.

For an incompressible Maxwell body, under constant stress the following equation applies[40,43]

$$k(t) = \frac{t}{\eta_M} + \frac{1}{E_M} \qquad (8)$$

which is simply its creep compliance function.[42] For purely Newtonian flow ($E_M \to \infty$), this expression can be simplified

to the kinetic relationship for viscous flattening with the Newtonian material viscosity η[40]

$$\left(\frac{x}{a} \right)^2 = \left(3 \cdot \frac{F_t}{a^2} \right)^{\frac{2}{3}} \cdot \left(\frac{t_H}{\eta} \right)^{\frac{2}{3}} \qquad (9)$$

As the elastic component acting against the deformation is neglected in Eq. 9, the contact zone diameter is bound to be overestimated. However, based on this equation, it can already be seen how important the effect of the material viscosity on the kinetics of the contact zone build-up is. A change of the rheological behavior, for instance via a variation of $T - T_g$ of the material, can thus trigger a faster and more pronounced contact zone development leading to stronger cohesion between particles and caking phenomena.

If a more accurate description of the flattening process is required, the material-specific function $k(t)$ should not be simplified and can be derived from modeling the rheological behavior of the material of interest in simple relaxation or creep tests. If the rheological parameters of, for example, a material with "delayed elasticity" are known, $k(t)$ is found to be[42]

$$k(t) = \frac{1}{E_1} + \frac{1}{E_2} \cdot \left(1 - e^{-\frac{t E_2}{\eta_D}} \right) \qquad (10)$$

Depending on the parameters $T - T_g$, contact time and compressive force or deformation, that is, set penetration of the particle surfaces, a transition from mere viscoelastic surface flattening to viscous flow sintering on a short time scale is possible. Viscous flow sintering is also considered one of the main causes for caking and responsible for the formation of interparticle bridges, which are expected to induce the highest bonding forces and consist of the actual amorphous substance.[2,4,9,44] These bridges are built when particles are brought into contact and atoms or molecules diffuse from the convex particle surface to an evolving concave sinter neck. For amorphous materials and polymers in general, sintering by viscous flow can be observed at the centre point of contact and on the curved surface of touching particles. The kinetics of coalescence are determined by material viscosity and particle size. Additionally, material transport can also take place in the vapor phase.[45,46]

When an external force is applied, the sintering process is accelerated as a function of the imposed stress.[2,25,45] Despite the relevance of pressure-assisted sintering causing caking effects in powder storage, there are not many models available that deal with the corresponding interparticle bridge growth kinetics. In addition, they are often highly simplified and only apply to ideal materials under several assumptions.[40]

One example, which has, however, been proven to describe experimental investigations well, is the equation for initial phase pressure sintering kinetics as developed by Rumpf et al.[40] The action of a total force is considered, which can be composed of an externally applied load like bulk material weight, van der Waals interactions, or both at the same time. For simplification, they assumed the temperature to be constant and a Newtonian sink flow pattern of the material at the particle contact. For creeping or Stokes flow at very small Reynolds numbers, that is, for low-fluid velocities and very large Newtonian viscosities, the solution of the Navier–Stokes equations for two spherical viscous particles can be written as[40]

$$\left(\frac{x_b}{a} \right)^2 = \left(\frac{16}{5} \cdot \frac{\gamma}{a} + \frac{8}{5 \cdot \pi} \cdot \frac{F_t}{a^2} \right) \cdot \frac{t_H}{\eta} \qquad (11)$$
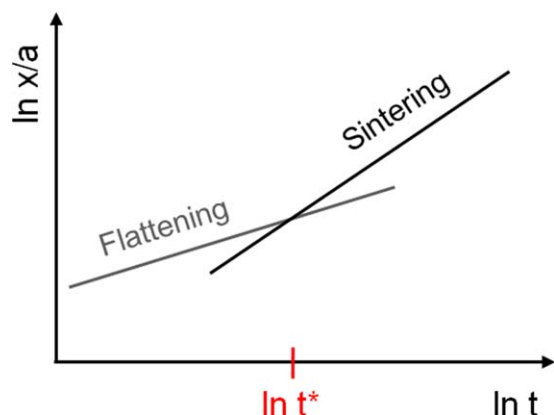
Figure 2. Schematic of transition from dominant viscous flattening to viscous sintering at a characteristic time *t** (based on[44]).

[Color figure can be viewed in the online issue, which is available at wileyonlinelibrary.com.]

The quantity x_b/a not only describes the normalized size of the sinter neck but also has a meaning for the degree of unwanted agglomeration. A "caking index" can be defined by dividing the diameter x_b of the bridges between individual particles by their size a. This can be related to different types of caking indices previously defined by other authors[4,14] such as the ratio between the porosity of the bulk powder after caking occurred and its initial porosity or the variation of the projected area of amorphous particles with time with respect to the projected area prior to the caking process.

According to Eq. 11, the material parameters viscosity η and surface tension γ influence the sintering kinetics for food particles as well as F_t. In the glass transition regime, the viscosity of the amorphous particles changes significantly and correspondingly also the sintering kinetics.

In the case of purely viscous sintering without elastic repulsive forces, a characteristic time t^* has so far only been defined theoretically[44] at which the diameter of both the contact area due to viscous flattening as well as the sinter neck are equal for the same applied force and material. For times smaller than t^*, flattening is the determining contact mechanism responsible for the development of the contact zone, whereas above t^*, sintering governs the particle interactions as can be seen in Figure 2.

t^* can be calculated by combining Eqs. 9 and 11[44]

$$\frac{t*}{\eta} = \frac{\left(3 \cdot \frac{F_t}{a^2}\right)^2}{\left(\frac{16}{5} \cdot \frac{\gamma}{a} + \frac{8}{5 \cdot \pi} \cdot \frac{F_t}{a^2}\right)^3} \tag{12}$$

t^* is only valid under the assumption of viscous flattening and sintering. This is the case for a certain physical state of the material under investigation, which is related to a high $T - T_g$ close to liquefaction. Also, the applied external forces and corresponding particle deformation have to be considered. For a fixed particle contact time, an increase of $T - T_g$ can thus bring about sintering instead of flattening as the dominant contact mechanism.

The theoretical construct described by Eq. 12 can be extended to the transition of viscoelastic instead of viscous flattening to sintering at lower $T - T_g$ values. In this case, however, the Newtonian viscosity of the substance is not sufficient to describe the deformation process of two spheres on load application and elastic repulsion also has to be considered. For a material with "delayed elasticity," the viscoelastic flattening model based on Eq. 7 using the expression for $k(t)$ in Eq. 10 can be combined with the relationship describing viscous sintering (Eq. 11) under load to deliver

$$\eta = \frac{t * \cdot \left(\frac{16}{5} \cdot \frac{\gamma}{a} + \frac{8}{5} \cdot \frac{F_t}{\pi \cdot a^2}\right)}{\left(\frac{3}{4 \cdot a^2} \cdot \left[\frac{1}{E_1} + \frac{1}{E_2} \cdot \left(1 - e^{-\frac{t * \cdot E_2}{\eta_D}}\right)\right] \cdot F_t\right)^{\frac{2}{3}}} \tag{13}$$

which does not give information about the characteristic time for the transition between the contact mechanisms. However, if desired, a force vs. η diagram can be established in which the required compressive force on a single particle of a defined size can be estimated, which is necessary to trigger sintering as the dominant contact mechanism in a set time interval. The latter can be considerably long, that is, several days or even months for caking probability estimations in a silo. With the WLF equation (Eq. 1), η can be related theoretically to the prevailing $T - T_g$ value of the material of the particles.

Material and Methods

A novel device called a MPT has been developed for the use in particle contact mechanism studies. Its setup, principles of operation and possible test procedures have been discussed in detail elsewhere[47] and only a short description is given here. In studies with the MPT, two particles with diameters above 500 μm can be forced into contact at a defined speed in a distance-controlled experiment while simultaneously recording the resulting compressive and tensile forces. This is achieved with the aid of a load cell (Honeywell Sensing & Control) with a detection limit of 1 N. It is possible to adjust the holding time in contact and record the force vs. time data, that is, a force relaxation curve. The novelty of the MPT lies in the possibility to adjust the temperature (10–45°C) and relative humidity (0–95% r.h.) of the test environment inside the measurement chamber, which is of critical importance for meaningful caking mechanism studies (Figure 3). The measurement chamber is sealed with a Perspex window to allow image or video capturing of the particles in contact to deliver information about the development of the interparticle contact zone diameter or bridge diameter with time. For this purpose, a Dino-Lite digital microscope AM-4013 manufactured by AnMo Electronics Corporation has been added to the setup and an automated Wolfram Mathematica 8 image analysis procedure has been developed.[47] The digital microscope is also used for the precise computer-assisted alignment of the two particles prior to bringing them into contact. The accuracy of the positioning procedure is further improved by a CCD camera at the bottom of the chamber, which displays the exact position of Particle 1 which is glued to a transparent glass window in a horizontally movable sample holder stage at the bottom of the measurement chamber. It has to be positioned below Particle 2 that is glued to a punch connected to the load cell and can only be moved vertically.

For the particle contact tests, spray-dried maltodextrin DE 21 (Glucidex 21, Roquette), a degradation product of maize starch, was selected as an amorphous model food powder. It is of great importance to the food industry due to its functionalities as a bulking agent, viscosifier, fat replacement, flavor carrier, and dispersing aid. For a DE value of 21, the
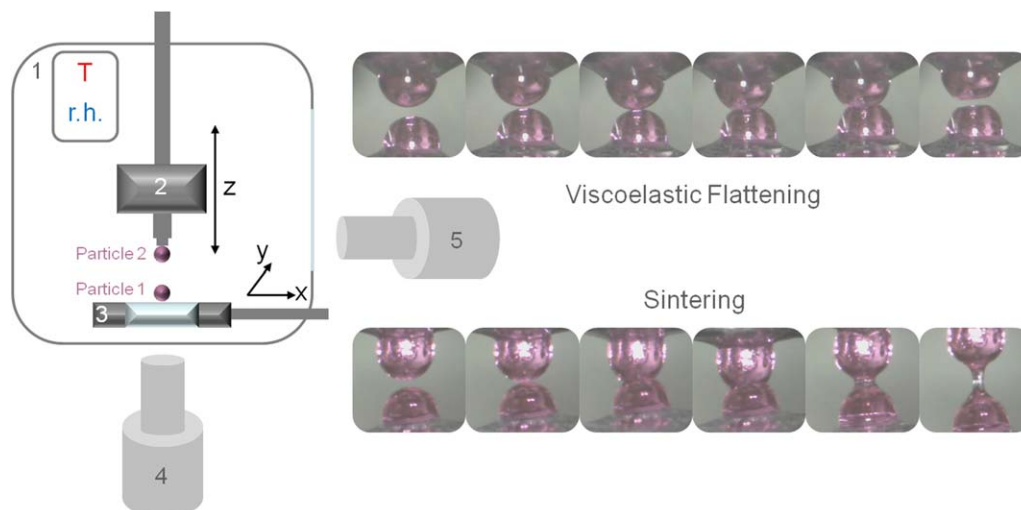
Figure 3. (1) MPT measurement chamber with controlled environment, (2) movable load cell and punch and (3) sample holder stage including glass window, (4) bottom-view camera, and (5) digital microscope.

Two image sequences of viscoelastic flattening and sintering as captured by (5) are shown. [Color figure can be viewed in the online issue, which is available at wileyonlinelibrary.com.]

glass transition temperature of this maltodextrin type lies between 20 and 60°C corresponding to a water activity range from 0.6 to 0.35. These values are similar to the majority of industrial food powder processes and storage conditions.[21,48,49] In addition, this model food material is always present in its amorphous form as its polydisperse nature inhibits the formation of an ordered supramolecular structure.[5]

To avoid the problems arising from irregular shapes and unknown roughness patterns of spray-dried particles (size range as determined by a QICPIC particle size and shape analyzer from Sympatec GmbH: 10^{-5}–10^{-3} m), a sample preparation method has been developed to produce well defined smooth maltodextrin DE 21 spheres of different sizes (RMS Rq roughness value just over $2 \times \cdot 10^{-9}$ m as determined by atomic force microscopy testing). In addition, theoretical models mostly assume that particles are spherical in shape, which means that the findings obtained from tests with the model spheres can directly be used for predictive calculations.

The developed method comprises the drying and solidification of droplets of highly concentrated dyed maltodextrin solution in an oil bath. Therefore, a viscous maltodextrin solution was prepared and mixed with a minute amount of the red colorant Erythrosin B (Acid Red 51). This enabled the identification of the particles during the manufacturing process and was also a prerequisite for an automated image analysis, which would not be possible for the otherwise translucent particles.[47]

The solution was broken down into spherical droplets in a warmed oil bath with the aid of magnetic stirrers. Subsequently, the water content of the droplets was reduced via drying until stable spherical beads with diameters between 1 and 1500 μm were created. Following this, the required size fraction of the particles was obtained via sieving and remainders of the oil were cleaned off with hexane before storing the beads in hermetically sealed plastic bags. A more detailed description of the procedure is given by Haider et al.[47]

Before the particles were used for contact tests, their size was determined by means of a stereomicroscope and pairs of similarly sized beads were selected. A small portion of the beads in the same size range were utilized for T_g determination using a DSC 1—differential scanning calorimeter from Mettler Toledo. The DSC results also gave proof of the complete removal of the oil from the particles as no crystallization peak was found. T_g double scans were, therefore, performed using a heating and cooling rate of 10°C/min. This rate of change in temperature can strongly affect the measured T_g value, which is found to be lower for slower DSC temperature scans, or higher for faster DSC temperature scans. This has to be borne in mind when comparing the results of this study for defined $T - T_g$ differences to the findings of other authors using different T_g measurement protocols. In addition, viscosity values calculated using the quantity $T - T_g$ (Eq. 1) have to be handled with care as they can differ strongly based on the T_g determination procedure used.

Based on the measured T_g, the corresponding $T - T_g$ could be adjusted inside the environmental chamber of the MPT. In principle, only the difference $T - T_g$ is relevant for the mechanical properties of the material independent of the individual values of T or T_g. This has been stated by other authors[8,19] and could also be proven in tests for which $T - T_g$ was kept constant for different combinations of T and T_g of maltodextrin DE 21 and similar results concerning compressive force and relaxation pattern were obtained. In the current study, however, the drying time of the particles was kept constant during production and only beads with a T_g of 23°C (within the limits of the accuracy of the DSC) were used.

To avoid drying or moisture uptake of the particles during a test, which would cause a change in $T - T_g$ and also the mechanical properties of the beads, the relative humidity in the environmental chamber of the MPT was set according to the water activity of the material.

Therefore, the relationship between the glass transition temperature, the water content, and the water activity of maltodextrin DE 21 was determined experimentally for selected a_W values generated by equilibration of powder samples at defined relative humidities. These were adjusted by a set of standard saturated salt solutions (lithium chloride, calcium

bromide, potassium acetate, magnesium chloride, potassium carbonate, magnesium nitrate, and sodium chloride—Sigma Aldrich). Subsequently, the BET model (Eq. 2) and the Gordon and Taylor equation (Eq. 3) were used to fit the measured data to be able to intrapolate the experimental findings to the physical state of the material of interest with a T_g of 23°C.

More precisely, the a_W values of the powder samples after equilibration were measured by means of a HygroLab C1 device, connected to sealed sample holder cells from Rotronic, at temperatures in the range of the used test conditions (21–39°C). The corresponding water content for each adjusted water activity was obtained gravimetrically by weighing the equilibrated powder samples before and after exposure for 2 h to a dry environment with P_2O_5 (Fluka Chemie AG, Switzerland) used as a desiccant under vacuum at 102°C to remove all contained water (method based on Vuataz[28]). To theoretically connect the water content (on dry basis) of the material with its water activity, that is, the relative humidity to be adjusted in the environmental chamber, the parameters n and m_m of the BET model (Eq. 2) were determined by fitting it to the experimental data. The optimized temperature-dependent parameters were, thus, found to be 22.28 for n and 4.51 for m_m at an intermediate temperature of 30°C.

The required empirical parameter k in the Gordon and Taylor equation (Eq. 3) was determined as 7.31 by curve-fitting based on the obtained glass transition temperatures of maltodextrin DE 21 using DSC for defined water activities and the related water contents (on wet basis). The parameter T_{gs} (152.9°C) was derived from DSC measurements on completely dehydrated maltodextrin DE 21 samples but can also be derived by extrapolating experimental data from moist samples to a water content of 0%.

Based on the findings and curve fits, additional maltodextrin DE 21 powder samples were equilibrated at 25°C in the environmental chamber of the MPT at a relative humidity of 0.61 or 61%, to generate a T_g of 23°C corresponding to the glass transition temperature of the beads used in the tests. Subsequent measurements in the Rotronic cells showed that also in this case the water activity of the powder did not vary considerably and remained approximately constant in the range of relevant environmental temperatures between 21 and 39°C. For this reason, a relative humidity of 61% was adjusted in the MPT measurement chamber for all contact tests.

Experimental

Two different test procedures were applied and all experiments were repeated at least three times for each combination of adjusted parameters. The first set of tests with the MPT focused on the effect of a change in $T - T_g$ on the dominant caking mechanism. In particular, the mechanical behavior of the maltodextrin DE 21 particle pairs and cohesion on their separation under the same environmental conditions as applied for the formation of a contact zone/sinter bridge, were investigated. The selected test conditions are summarized in Table 1. The deformation is based on the diameter of the undeformed spherical beads as measured with the stereomicroscope. Deformation, holding time, and test speed for approach and retract path of Particle 2 (Figure 3) were kept constant in all conducted tests. Prior to the actual tests, all pairs of beads were given a time span of 30

Table 1. Summary of the Conditions Applied in the First Set of Tests: $T - T_g$, T, Relative Humidity r.h., Deformation, Contact Holding Time t_H, and Test Speed

$T-T_g$ (°C)	T(°C)	r.h. (%)	Deformation (%)	t_H(s)	Test speed (m/s)
5.5	28.5	61	10	3	10^{-4}
6.5	29.5	61	10	3	10^{-4}
8.5	31.5	61	10	3	10^{-4}
14	37	61	10	3	10^{-4}

min (1800 s) to equilibrate with the adjusted temperature T inside the environmental chamber. Even shorter equilibration times were proven to be sufficient based on images of the tempered chamber and the enclosed particles taken with a thermal imaging camera. They showed an almost immediate matching of color and, thus, temperature between introduced beads and the adjusted environmental conditions inside the chamber.

A second set of tests was performed to investigate in which way the strength of a sinter bridge could be influenced by alterations of the temperature. A $T - T_g$ of 16°C (similar test conditions as stated in Table 1) was adjusted leading to an immediate formation of a material bridge. Subsequent cooling over a range of 18 from 39°C to 21°C brought the bridge and particles into the glassy state ($T - T_g = -2$°C). After a total of 45 min (2700 s), for cooling as well as equilibration of the material with the decreased temperature of 21°C, the bridge was ruptured at a speed of 10^{-4} m/s to record the breakage force.

Results and Discussion

Experiments for short holding times at constant deformation and positive values of the difference $T - T_g$ have been performed to study the transition from viscoelastic flattening and enhanced stickiness of maltodextrin DE 21 particles to sintering. The effect of a temperature change on the contact zone growth and actual interparticle cohesion was also explored.

Three different $T - T_g$ values (5.5, 6.5, and 8.5°C) triggering the occurrence of viscoelastic flattening have been investigated concerning the behavior of similarly sized maltodextrin beads (~800 μm) under a constant 10% deformation for contact holding times of 3 s. The recorded relaxation curves give information about the change in the rheological behavior of individual amorphous particles due to variations of the quantity $T - T_g$, which determines the balance of their viscous and elastic properties.

Typical examples of selected force vs. time trajectories as directly obtained from the MPT measurements are displayed in Figure 4. For applying the same deformation of 10% in a distance-controlled particle contact experiment, different initial maximum compressive forces are obtained ranging from around 0.6 N for a $T - T_g$ of 5.5°C to approximately 0.1 N for 8.5°C. Maltodextrin DE 21 obviously becomes less stiff with rising $T - T_g$ values. This can also be derived from the decreasingly steep slope of the force-time curve up to the detected maximum force for a constant deformation velocity. After the viscoelastic particles in contact reach the maximum compressive force on a deformation of 10%, they relax in different patterns according to their $T - T_g$. The particles
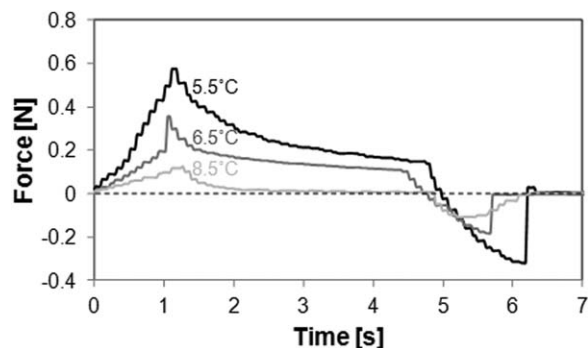
Figure 4. Example curves for selected interparticle tests for different states of the material ($T - T_g = 5.5$, 6.5, and $8.5°C$) at a holding time of 3 s and a deformation of 10% (environmental conditions: see Table 1).

Figure 5. Schematic overview of compressive and cohesion force trends for different positive $T - T_g$ values and summary of mechanical interactions occurring.

[Color figure can be viewed in the online issue, which is available at wileyonlinelibrary.com.]

behave quite viscously for a $T - T_g$ of $8.5°C$, which is clearly observed in their fast relaxation to a zero force state. The energy introduced by compressive deformation is most probably quickly dissipated into the flattening of the particle surfaces and the formation of a contact zone. At a $T - T_g$ of $6.5°C$, the material does not relax to zero during the holding time of 3 s, but approaches a finite value of approximately 0.15 N, which indicates that compressive positive-valued stresses are still acting between the particles on their separation occurring when Particle 2 is moved upward (Figure 3). More time is obviously necessary for a relaxation of the applied compressive stress resulting in particle deformation.

Lowering $T - T_g$ to $5.5°C$ triggers an even slower relaxation, which is not completed within the short deformation holding time applied in the experiment, leading to the highest remaining compressive force on particle separation.

The recorded induced bonding forces exhibit negative values due to their opposing orientation in comparison to the compressive forces. It is found that the cohesion between the particles decreases the softer the material becomes (higher $T - T_g$). For the lowest tested $T - T_g$ of $5.5°C$, a blunt rupture of the touching particle surfaces (see microscope images adjacent to Table 2) on retraction is observed. This is accompanied by the strongest detected pull-off force and represents an apparent "optimum condition for cohesion."

Tests on particles with even lower positive $T - T_g$ values of $4°C$ (not displayed in Table 2) prove to deliver maximum compressive forces larger than 1 N that were outside the limits of the load cell and showed decreasing cohesion values
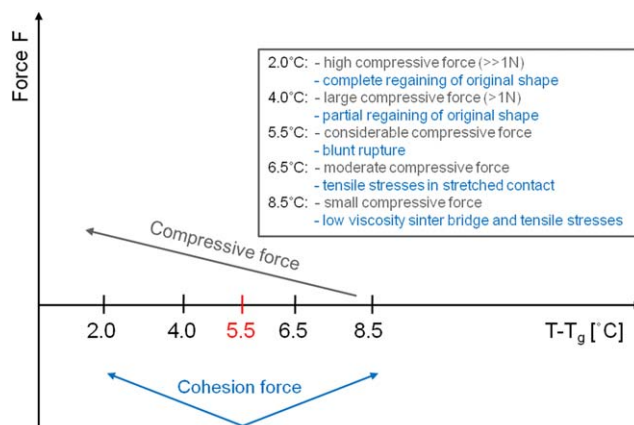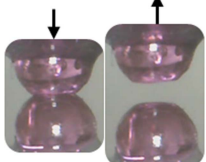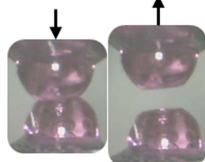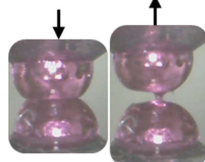
even for an extended holding time of 10 s (measured cohesion: -0.1 N). Eventually, for a $T - T_g$ of $2°C$, bonding forces could no longer be measured. This extends the statement made by other authors, for example, Aguilera,[4] that no caking is observed for free flowing amorphous powders in their glassy state, to the current case of amorphous powders at the onset of their rubbery state for this size class of particles and short contact times. In addition, the worst caking due to viscoelastic flattening is correspondingly to be expected for $T - T_g$ values around $5.5°C$, which is also highlighted in the schematic overview in Figure 5.

This is most likely due to the remaining compressive forces in the contact zone on particle separation. They can act in favor of cohesion based on van der Waals interactions by pushing the permanently flattened particle surfaces together when one particle is withdrawn and, thus, facilitating a large contact zone when the observed blunt rupture occurs. This stands in contrast to a gradual peeling-off type of disconnection, which is found for stiffer particles (e.g., for a $T - T_g$ of $4°C$). In this case, the particles partly recover their spherical shape while they are separated and the contact zone reduces gradually before the final surface disconnection.

The drop in cohesion observed for a $T - T_g$ value of $6.5°C$ can be explained by the softening of the material and the increased deformability of the maltodextrin beads. On

Table 2. Averaged Maximum Compressive and Cohesive Forces as a Function of $T - T_g$ for a 10% Deformation Holding Time of 3 s for the Three Examples Shown in Figure 4 Including Images Taken with the Digital Microscope of Particles in Contact and After Disconnection of the Surfaces [Color table can be viewed in the online issue, which is available at wileyonlinelibrary.com]

$T - T_g (°C)$	5.5	6.5	8.5
Max. compressive force (N)	0.61	0.39	0.13
Cohesive force (N)	−0.22	−0.16	−0.09

withdrawal of one particle, the cohesion between the bead surfaces is most probably strong enough to cause a stretching of the softened particle material perpendicular to the contact area before separation occurs. This can lead to internal tensile stresses, which diminish the overall cohesion (Figure 5).

Enhancing $T - T_g$ to even higher values such as 8.5°C induces a transition from mere flattening to the onset of sintering with the build-up of small low-viscosity material bridges in the contact zones between the particles (see microscope images adjacent to Table 2).

Due to the quite stable particle structure and measured resistance to deformation, the occurrence of sintering is surprising under the prevailing conditions in the environmental chamber. It can most probably be related to the onset of capillary condensation, where surface roughnesses come into close proximity, especially around the centre of contact zone between the particles. This softens the material locally and supports sintering leading to the build-up of the observed plasticized, that is, low viscosity, material bridge. The latter does not add considerably to the recorded cohesive tensile force resulting in the smallest detected cohesion of the particles (Figure 5).

Considering the little compressive forces of approximately 0.13 N experienced by the material under the fixed deformation of 10%, it is possible that the particles in a powder bulk would collapse for a $T - T_g$ of 8.5°C if a sufficient load is applied, for example, the weight force of a powder layer in a storage facility.

For sintering to become the dominant contact mechanism in a distance-controlled experiment, longer contact times or lower material viscosities are required than induced by a $T - T_g$ of 8.5°C. This was shown experimentally and can also be confirmed theoretically using Eq. 12 to estimate the critical time necessary for the sinter bridge diameter being equal to the diameter of the flattened contact zone. Estimating the viscosity of maltodextrin DE 21 with the aid of the WLF relationship (Eq. 1) using the universal parameters and assuming a viscosity of 10^{12} Pa.s close to the glass transition temperature delivers values of 2.1×10^{10} Pa.s $(T - T_g = 5.5°C)$, 1.1×10^{10} Pa.s $(T - T_g = 6.5°C)$, and 3.5×10^9 Pa.s $(T - T_g = 8.5°C)$. The, thus, calculated critical time for dominant sintering in the three tested physical states of maltodextrin is several magnitudes higher than the imposed contact time of 3 s, even if an enhanced external force of 1 N is considered. The calculated viscosity values have, however, not been proven to apply to this particular testing material, in particular regarding the estimated viscosity in the glassy state and the use of the universal constants, which might not hold for hygrosensitive amorphous substances such as maltodextrin DE 21. Moreover and as mentioned earlier in "Material and Methods," the procedure used for the T_g determination strongly affects the obtained $T - T_g$ value. This in turn can lead to large variations in the estimated viscosity based on the WLF approach. To make results of different researchers concerning the expected material viscosity comparable, the $T - T_g$ values obtained by DSC can be "adapted" according to the measurement protocol used.

To generalize the interpretation of the compressive and cohesion force results independent of slight variations in the particle diameters used for different tests, the size of the contact zone based on the diameters obtained with the digital microscope and the recorded force data can be combined to deliver information about the stress state of the particles and
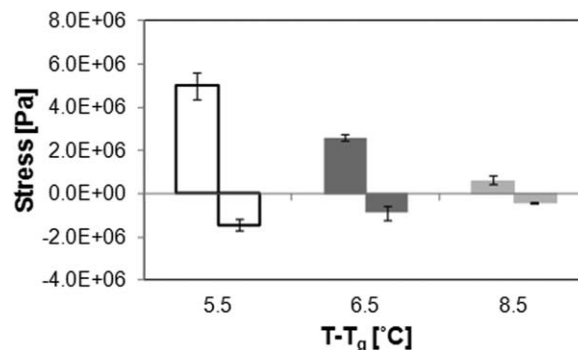

Figure 6. Averaged maximum compressive stress and bonding strength as a function of $T - T_g$ for a 10% deformation holding time of 3 s for the three examples shown in Figure 4.

Each mean value is based on a set of at least three tests.

the resulting bonding strength (Figure 6). The bonding force values in Figure 4 and Table 2 are only applicable for the particle size used in a particular test.

In addition to the relevance of the optically measured contact zone size for the derivation of the actual stress state of the particles from the force vs. time data, its development as a function of the holding time is of great interest. It can give important indications concerning the densification of a bulk powder when its porosity is decreased during a defined storage period due to particle deformation and the development of larger interparticle contact zones reducing the initial void spaces between them. The measured averaged ratio x/a, which is the contact zone diameter normalized with the particle size, is plotted against time in Figure 7 based on at least three tests for each $T - T_g$, whereas the averaged maximum ratios measured after 3 s in all conducted trials are shown in Figure 8.

Due to the soft character of the material at the highest $T - T_g$ of 8.5°C, the deformation is more pronounced, that is, x/a is found to be large, which can be seen both in the x/a vs. time data in Figure 7 as well as in the averaged maximum contact zone diameters in Figure 8. Correspondingly, smaller contact zone sizes are induced when lowering the difference of $T - T_g$. Hereby, the higher viscosity and elastic repulsion act against the deformation and reduce the size of the contact zone.

Interestingly, the stiffest particles at a $T - T_g$ of 5.5°C deliver the largest cohesion despite showing the smallest contact zone on separation. In addition, an ongoing growth of the contact zone is observed, which is related to the incomplete continuous relaxation of the material (see Figure 4). During the holding time, the remaining compressive energy is dissipated into further deformation and contact zone growth. A slight increase of the contact area diameter over time can also be observed for the case of $T - T_g = 6.5°C$, which is again related to its relaxation pattern. The softest particles with a $T - T_g$ of 8.5°C exhibit an instantaneous remnant deformation and the diameter of the contact zone between them only shows a negligible increase during the holding time. Based on the quick relaxation to a zero force or stress state in this case, there is little potential for further contact zone growth during the short contact of 3 s. Due to this, no additional van der Waals interactions can take place to enhance cohesion. However, for longer holding times, as applicable to storage of food powder, time-
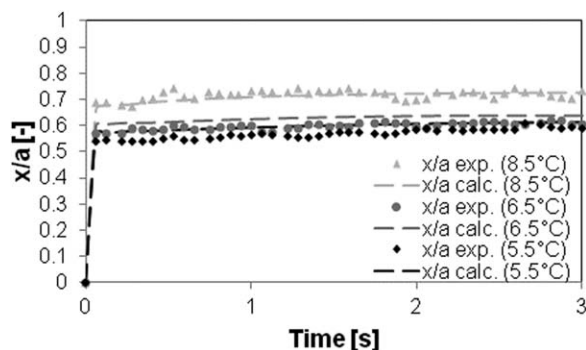
Figure 7. x/a ratios for an initial holding time period of 3 s at a deformation of 10% for three different tested $T - T_g$ values within the viscoelastic regime (5.5, 6.5, and 8.5°C) in comparison to the theoretical results from the adapted kinetics model (Eq. 7 in combination with Eq. 10) based on Wei Hsuin.[43]

Figure 8. Summarized maximum ratios of x/a after a holding time of 3 s as a function of $T - T_g$ (5.5, 6.5, and 8.5°C).

dependent sintering becomes the dominant contact or caking mechanism depending on the environmental conditions and forces acting on individual particles. The bonding strength is then mainly determined by the bridge material properties.

It has to be noted that the formation of a large contact zone due to an enhanced softness of an amorphous material can cause even worse caking problems when the environmental conditions fluctuate to lower $T - T_g$ values afterward. A large contact zone in combination with the optimum physical state for interparticle cohesion can trigger severe caking effects. In addition, the performed experiments are position-controlled and the resistance of the material to a certain fixed deformation (10%) is investigated. For storage of powder, the applied force on the particles has a constant value depending, for example, on the position of the particles in a silo and the weight force of the powder layers above. It can easily be seen in Figure 4 that softer particles are less resistant to applied force, that is, they experience lower compressive forces on a certain deformation than stiffer "drier" particles. This confirms the formation of even larger contact zones and enhanced deformation of particles with high $T - T_g$ values in comparison to particles at the onset of glass transition or in their glassy state with low or negative $T - T_g$ differences when a constant force is applied.

In addition to the experimental observations, the contact zone development was also described theoretically. For this purpose, the equation based on Wei Hsuin[43] (Eq. 7) was used to take into account how the relationship between elastic repulsion and viscosity determines the time-dependent contact diameter growth. The observations on a short time scale concerning the formation of the flattened area between two particles can, thus, be extrapolated to longer contact times as applicable to most industrial powder storage situations. Furthermore, Eq. 7 is based on a constant load being exerted on the particles, which is closer to reality where a certain weight force of, for example, a powder layer in a silo, acts on particles.

It was found that the relaxation behavior of maltodextrin DE 21 particles can be described using the differential equation related to a material with "delayed elasticity" (Eq. 5). Correspondingly, the parameters E_1, E_2, and η_D, which are necessary for Eq. 7 and the material-specific creep function of the material of interest (see Eq. 10) can be obtained.
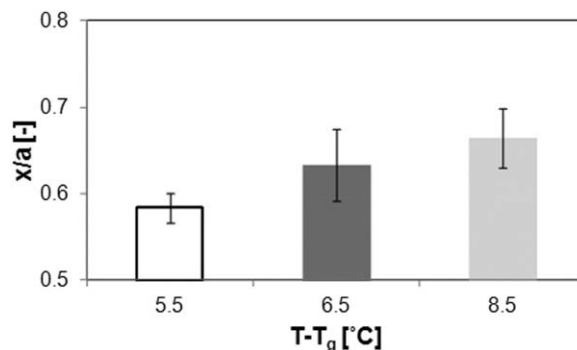
These parameters accurately describe the elastic as well as viscous properties of maltodextrin DE 21 in different physical states. It thereby has to be noted that the dashpot or viscosity parameter η_D is not equal to the Newtonian viscosity η.

The required stress relaxation curves were obtained by relating the size of the contact zone, based on the measured diameters, and the recorded force as a function of the holding time for all captured data during the contact period. The viscoelastic parameters resulting from fitting these relaxation curves with Eq. 5 are displayed in Table 3.

The viscoelastic parameters could directly be used in Eq. 7 to estimate the contact zone development between two particles at the three different tested $T - T_g$ values for application of a constant load. For the distance-controlled MPT studies, however, the kinetics model had to be slightly modified to account for the changing compressive load due to relaxation mechanisms. A balance of forces was assumed for simplification. The force introduced to the particle-particle system over time by means of the total acting compressive force was believed to be approximately equal to the dissipation force leading to a deformation of the particle surfaces. A change in temperature due to frictional heat was thereby considered negligible due to the low force acting on the system over time. This force was calculated by the formation of a simple integral over the measured forces $F(t)$ and the elapsed contact time at the current holding time value. This corresponds to the summation of force-time intervals as obtained from the experimental data or, basically, to the area under the force-time curve. Subsequently, an average force, which acts on the system up to the point of interest, was calculated by dividing this area by the current holding time value and used instead of $F(t)$. This approach, using a stepwise integration and averaged force values, might not account for the development of the compressive force over

Table 3. Viscoelastic Parameters (E_1, E_2, and η_D) as Obtained from Stress Relaxation Curves Measured Between Maltodextrin DE 21 Particles Under a Constant Deformation of 10% in Varying Physical States ($T - T_g = 5.5$, 6.5, and 8.5°C)

$T - T_g$(°C)	E_1(Pa)	E_2(Pa)	η_D(Pa.s)
5.5	$4.7 \cdot 10^6$	$2.1 \cdot 10^6$	$7.9 \cdot 10^6$
6.5	$2.4 \cdot 10^6$	$1.0 \cdot 10^6$	$2.9 \cdot 10^6$
8.5	$7.9 \cdot 10^5$	$4.8 \cdot 10^4$	$4.5 \cdot 10^5$

time. However, it poses a simplified approach to estimate the contact zone diameter between particles for a fixed-grip, that is, distance-controlled, experiment and is tested against the actually recorded data.

Care has to be taken at the point where the compressive force relaxes to zero or to a finite value close to zero. From this holding time value onward, the contact zone diameter between the flattened particles can be considered constant unless a contact mechanism of a different nature, like sintering, based on a driving force other than external pressure, is observed over time. For particles with a low-viscosity and high-molecular mobility, the tendency of the free surface energy to drive a reduction of the overall surface area of the particles can lead to material flow into the contact zone already at short contact times (depending on the actual $T - T_g$ of the material—compare experiments at 8.5°C) and the formation of interparticle bridges following a different time law.

The results of three sets of experiments applying a fixed deformation of 10% on rubbery particles with $T - T_g$ values of 5.5, 6.5, and 8.5°C in comparison with their modeled contact zone diameters are shown in Figure 7. For the three different studied physical states and the imposed deformation of 10%, very good results are achieved; although the fixed-grip-type experiment hinders a further approach of the particle centre points, that is, creep of the material, which would even lead to larger contact zones if a constant force was applied over time.

Even if relaxation occurs quickly leading to a fast change in the compressive force, the assumption of an averaged force over time holds well. Although sintering occurs at a $T - T_g$ of 8.5°C, its effect on the contact zone formation is obviously still negligible and the model continues to describe the resulting flattened area between the particles well.

Based on the experimentally obtained viscoelastic parameters of maltodextrin DE 21 (Table 3), Eq. 13 could now also be used for some model calculations to estimate the transition from flattening to sintering as the dominant contact mechanism. Instead of estimating a critical time value, the contact time was taken to be 3 s and the limiting Newtonian viscosity for dominant sintering, which is the relevant parameter for viscous sintering, was calculated and compared to the WLF predictions for different $T - T_g$ values. As a result, the prerequisite viscosities for dominant sintering at this short time scale and under low compressive forces in the range of 1 N were about four magnitudes lower than the viscosities predicted with the WLF approach. This might not be a highly accurate statement due to the uncertainties concerning the WLF parameters and theoretical viscosity close to the glassy state of 10^{12} Pa.s as well as the used technique to determine T_g experimentally. However, due to the large difference between the required viscosities for dominant sintering and the estimated WLF viscosities, it can be assumed that the error in the calculated viscosities does not exceed four orders of magnitude. Correspondingly, the real viscosity of maltodextrin DE 21 is also expected to be too high to trigger sufficient molecular mobility, that is, material flow and the build-up of sinter bridges that are larger than the flattened contact zones.

Finally, sintering as the dominant contact mechanism has also been investigated considering the acting forces and the implications for caking. A $T - T_g$ of 14°C was chosen to generate a low material viscosity as a prerequisite for instantaneous predominantly viscous sintering that would lead to a
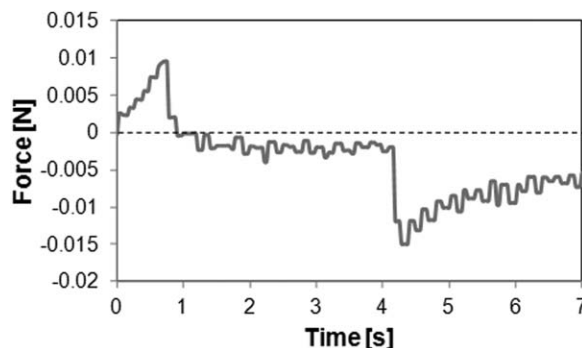

Figure 9. Example curve for interparticle sintering tests at a $T - T_g$ of 14°C and a deformation of 10% holding time of 3 s (environmental conditions: see Table 1).

collapse of the powder structure and loss of particle shape. For this physical state of the material, the detection limits in terms of measurement sensitivity of the used load cell in the MPT are reached and the recorded force vs. time signal in Figure 9 shows fluctuations within its accuracy levels. A very low compressive force of approximately 0.01 N (compressive stress: 0.02 MPa) was measured, with the bonding force based on the strength of the material bridge being in the same order of magnitude with a value of approximately 0.015 N (tensile strength: 0.04 MPa). Due to the almost liquid-like behavior of maltodextrin DE 21 under the prevailing environmental conditions and the corresponding low viscosity, only minute forces are required for fusing the particles and creating a material bridge of considerable size. The automated image analysis shows that a ratio x/a (x = bridge diameter) of around 0.7 is reached immediately after the particles are brought into contact at a deformation of 10%, which remains constant throughout the holding time of 3 s. However, the bridge is not very strong and does not rupture on withdrawal of Particle 2 (see Figure 3) up to the maximum movement range of the load cell and punch inside the MPT environmental chamber. This can be seen in Figure 9, where the negative-valued bonding force of the bridge gradually decays due to a thinning of the stretched material bridge.

As pointed out earlier, sintering is expected to be the main contact mechanism between particles leading to caking and the issues connected to it. Obviously, low-material viscosity and particle fusion based on viscous sintering lead to the collapse of a powder bed without the necessity of large compressive forces. In contrast to this, no enhanced interparticle cohesion can be observed in these cases due to the weakness of the material on stretching/extension. In industrial reality, however, fluctuations of the temperature and humidity of the environment are very common. For occasional temperature rises and enhanced relative humidity of the air, the stored powder can enter glass transition and sintering can be triggered. In subsequent drops of both temperature and relative humidity, the sintered powder might return to its glassy state including the previously formed material sinter bridges. This process has been simulated in the MPT to investigate the effect of strong temperature and humidity fluctuations in powder processing and storage.

After instantaneous sintering of maltodextrin beads at the highest $T - T_g$ of 16°C for maintaining their spherical shape, the environmental chamber of the MPT was cooled down to
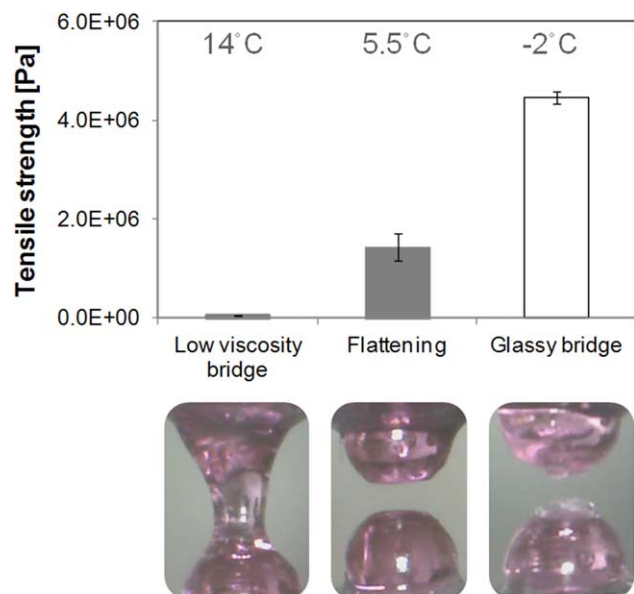
Figure 10. Top: Comparison of the tensile strength of a low-viscous bridge and a brittle glassy bridge to the bonding strength based on viscoelastic particle flattening (applied deformation: 10% in all cases, tensile/bonding strength plotted with positive values).

Bottom: Corresponding images of the particles on retraction. [Color figure can be viewed in the online issue, which is available at wileyonlinelibrary.com.]
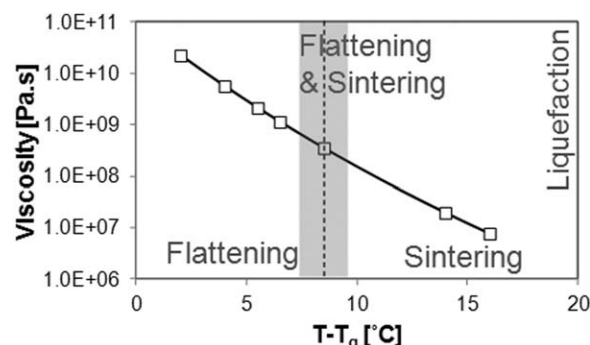

Figure 11. Viscosity values calculated using Eq. 1 for pure flattening, the onset of sintering overlapping with particle deformation and dominant sintering as a function of $T - T_g$ (highlighted for 2, 4, 5.5, 6.5, 8.5, 14, and 16°C) for a short holding time of 3 s.

create a negative difference between T and T_g of -2°C, that is, to bring the particles and the bridge into the glassy state without disconnecting them. Subsequently, the glassy bridge was ruptured to detect its strength and showed a brittle fracture pattern on moving Particle 2 upward. The averaged tensile strength of the glassy material bridges is shown in Figure 10 in comparison to the cohesion caused by flattening ($T - T_g$ of 5.5°C) and the strength of the low-viscosity bridge under the $T - T_g$ setting of 14°C.

Sinter bridges can obviously gain a high-tensile strength on changes of the physical state of the powder material from rubbery to glassy.

Conclusions

Contact experiments between individual amorphous hygrosensitive model food particles in a controlled environment have been conducted and have delivered valuable information about caking mechanisms. For a short holding time of 3 s, viscoelastic flattening could be observed for positive $T - T_g$ values up to 8.5°C in combination with cohesion forces that are most likely induced by van der Waals interactions. Based on the recorded relaxation curves in the distance-controlled experiments, it was also found that increased values of $T - T_g$ induce softening of the material, that is, a drop in viscosity, and the formation of larger contact zones between the deformed particles in the flattening regime. This behavior was described theoretically by fitting stress relaxation curves of maltodextrin DE 21 particles with a three parameter viscoelastic model and subsequently using the obtained rheological parameters for a prediction of the contact zone formation under load as a function of time. The relationship based on Wei Hsuin[43] delivered normalized con-

tact diameters that described the experimental data well. It is now possible to theoretically predict the size of contact zones between flattened particles if the relevant process parameters are known.

Despite a monotonous growth of the contact zone concomitant with an augmentation in the parameter $T - T_g$, the measured cohesion on particle disconnection was shown to increase to its apparent maximum at approximately 5.5°C above T_g for an elevation of the environmental temperature, but to decrease again after further heating. This can most likely be related to the stretching of the increasingly soft material around the contact zone on retraction and the connected tensile stresses inside the particles acting in favor of separation. For $T - T_g$ differences in the proximity of 8.5°C (area shaded in grey in Figure 11), the onset of viscous sintering can be observed at the investigated short holding time. The formed material bridges are, however, very weak due to their low viscosity and are most probably the result of a localized plastification process in the particle contact zone triggered by capillary condensation. In addition, their diameter is small in comparison to the flattened contact zone size.

On further heating, sintering is found to be the dominant contact mechanism for the investigated $T - T_g$ values of 14 and 16°C. Due to the strong influence of the applied T_g measurement technique on the quantity $T - T_g$, care has to be taken when comparing these findings to the results of other researchers.

To investigate the effect of temperature changes that can occur during the storage of powder, tests have been performed simulating a rise in temperature up to instantaneous sintering conditions in the rubbery, almost liquid-like state of the model particles. A subsequent drop of the temperature toward negative values of $T - T_g$ was then introduced translating into a glassy state of both beads and formed bridges. The latter were then ruptured to measure their tensile strength with the result of stronger interparticle bonding than measured in all contact tests with short holding times for the investigated environmental conditions between a $T - T_g$ of 2°C and 16°C outweighing even the apparent optimum cohesion conditions for flattening at 5.5°C.

The strength of interparticle bridges has, thus, been shown to be quantitatively determinable with the aid of the MPT. Many different heating/cooling and relative humidity ramps can be tested on various amorphous materials within the

limits of adjustable conditions inside the environmental chamber of the MPT. For instance, short increases in the relative humidity can be applied to plasticize only the particle surface to mirror a sintering process without complete collapse in a silo.

In general, particle pair tests are of great importance as small differences of, for example, environmental parameters, and thus, $T - T_g$ of amorphous substances can lead to very different caking mechanisms and resulting strength of the agglomerated powder that cannot be explained by bulk material studies. The parameters applied to a powder in an industrial process can be broken down to a particle-particle level to tailor the test conditions including forces acting on them due to air flow, agitation, or bulk weight force. This delivers indispensable information for predictive modeling of unwanted agglomeration processes.

Acknowledgments

Literature Cited

1. Palzer S. Agglomeration of dehydrated consumer foods. In: Salman AD, Hounslow MJ, Seville JPK, editors. *Handbook of Powder Technology—Granulation*, Vol. 11. Amsterdam: Elsevier, 2007.
2. Hartmann M, Palzer S. Caking of amorphous powders—material aspects, modelling and applications. *Powder Technol.* 2011;206(1–2):112–121.
3. Christakis N, Wang J, Patel MK, Bradley MSA, Leaper MC, Cross M. Aggregation and caking processes of granular materials: continuum model and numerical simulation with application to sugar. *Adv Powder Technol.* 2006;17(5):543–565.
4. Aguilera JM, del Valle JM, Karel M. Caking phenomena in amorphous food powders. *Trends Food Sci Technol.* 1995;6(5):149–155.
5. Fitzpatrick JJ, Descamps N, O'Meara K, Jones C, Walsh D, Spitere M. Comparing the caking behaviours of skim milk powder, amorphous maltodextrin and crystalline common salt. *Powder Technol.* 2010;204(1):131–137.
6. Mathlouthi M, Roge B. Water vapour sorption isotherms and the caking of food powders. *Food Chem.* 2003;82(1):61–71.
7. Wahl M, Brockel U, Brendel L, Feise HJ, Weigl B, Röck M, Schwedes J. Understanding powder caking: predicting caking strength from individual particle contacts. *Powder Technol.* 2008;188(2):147–152.
8. Foster KD, Bronlund JE, Paterson AHJ. Glass transition related cohesion of amorphous sugar powders. *J Food Eng.* 2006;77(4):997–1006.
9. Cleaver JAS, Karatzas G, Louis S, Hayati I. Moisture-induced caking of boric acid powder. *Powder Technol.* 2004;146(1–2):93–101.
10. Levi G, Karel M. Volumetric shrinkage (collapse) in freeze-dried carbohydrates above their glass transition temperature. *Food Res Int.* 1995;28(2):145–151.
11. Dupas-Langlet M, Benali M, Pezron I, Saleh K, Metlas-Komunjer La. Deliquescence lowering in mixtures of NaCl and sucrose powders elucidated by modeling the water activity of corresponding solutions. *J Food Eng.* 2013;115(3):391–397.
12. Langlet M, Benali M, Pezron I, Saleh K, Guigon P, Metlas-Komunjer La. Caking of sodium chloride: role of ambient relative humidity in dissolution and recrystallization process. *Chem Eng Sci.* 2013;86(0):78–86.
13. Karel M, Anglea S, Buera P, Karmas R, Levi G, Roos Y. Stability-related transitions of amorphous foods. *Thermochim Acta.* 1994;246(2):249–269.
14. Saragoni P, Aguilera JM, Bouchon P. Changes in particles of coffee powder and extensions to caking. *Food Chem.* 2007;104(1):122–126.
15. Listiohadi Y, Hourigan JA, Sleigh RW, Steele RJ. Moisture sorption, compressibility and caking of lactose polymorphs. *Int J Pharm.* 2008;359(1–2):123–134.
16. Renzetti S. Water migration mechanisms in amorphous powder material and related agglomeration propensity. *J Food Eng.* 2012;110(2):160–168.
17. Ferry JD. Viscoelastic Properties of Polymers, 3rd ed. New York: Wiley, 1980.
18. Sperling L. Introduction to Physical Polymer Science. New York: Wiley, 1986.
19. Williams ML, Landel RF, Ferry JD. The temperature dependence of relaxation mechanisms in amorphous polymers and other glass-forming liquids. *J Am Chem Soc.* 1955;77:3701–3707.
20. Fox TG, Flory PJ. Second-order transition temperatures and related properties of polystyrene. I. Influence of molecular weight. *J Appl Phys.* 1950;21(6):581–591.
21. Palzer S. Agglomeration of Food Powders. Habilitationsschrift. Munchen: Technische Universitat Munchen, 2007.
22. Palzer S. Influence of material properties on the 965 agglomeration of water-soluble amorphous particles. *Powder Technol.* 2009;189(2):318–326.
23. Miguel AF. Effect of air humidity on the evolution of permeability and performance of a fibrous filter during loading with hygroscopic and non-hygroscopic particles. *J Aerosol Sci.* 2003;34(6):783–799.
24. Labuza TP, Altunakar B. Water activity prediction and moisture sorption isotherms. In: Barbosa-Canovas GV, Fontana AJ, Schmidt SJ, Labuza TP, editors. *Water Activity in Foods: Fundamentals and Applications.* Oxford: Blackwell Publishing Professional, 2007.
25. Palzer S. The effect of glass transition on the desired and undesired agglomeration of amorphous food powders. *Chem Eng Sci.* 2005;60(14):3959–3968.
26. Brunauer S, Emmett PH, Teller E. Adsorption of gases in multimolecular layers. *J Am Chem Soc.* 1938;60(2):309–319.
27. Weisser H. Influence of the temperature on sorption isotherms. In: Maguer M, Jelen P, editors. *Transport Phenomena.* New York: Elsevier Science, 1986.
28. Vuataz G. The Phase Diagram of Milk: *A New Tool for Optimising the Drying Process,* In Le Lait - Dairy Science and Technology, Vol. 82. 2002:485–500.
29. Roos Y. *Phase Transitions in Foods.* San Diego: Elsevier, 1995.
30. Duffrene L, Gy R, Burlet Hln, Piques R, Faivre A, Sekkat A, Perez J. Generalized Maxwell model for the viscoelastic behavior of a soda-lime-silica glass under low frequency shear loading. *Rheol Acta.* 1997;36(2):173–186.
31. Labuza TP. Sorption phenomena in food. *Food Technol.* 1968;22(3):263–272.
32. Karel M. Physico-chemical modifications of the state of water in foods: a speculative survey. In: Duckworth RB, editor. *Water Relations of Foods.* London: Academic Press, 1975.
33. Van den Berg C, Bruin S. Water activity and estimation in food systems. In: Rockland LB, Stewart GF, editors. *Water Activity: Influences on Food Quality.* New York: Academic Press, 1981.
34. Jouppila K, Roos YH. Glass transitions and crystallization in milk powders. *J Dairy Sci.* 1994;77(10):2907–2915.
35. Gordon M, Taylor JS. Ideal copolymers and the second-order transitions of synthetic rubbers. i. Non-crystalline copolymers. *J Appl Chem.* 1952;2(9):493–500.
36. Attard P. Interaction and deformation of viscoelastic particles:1. Nonadhesive particles. *Phys Rev E.* 2001;63(6):061604.
37. Hamaker H. The London—Van der Waals attraction between spherical particles. *Physica.* 1937;4(10):1058–1072.
38. Butt H-J, Kappl M. *Surface and Interfacial Forces.* Weinheim: Wiley-VCH Verlag, 2010.
39. Attard P. Interaction and deformation of viscoelastic particles. 2. Adhesive particles. *Langmuir.* 2001;17:4322–4328.
40. Rumpf H, Sommer K, Steier K. Mechanismen der Haftkraftverstarkung bei der Partikelhaftung durch plastisches Verformen, Sintern und viskoelastisches Fließen. *Chem-Ing-Tech.* 1976;4:300–307.
41. Barnes H, Hutton J, Walters K. *An Introduction to Rheology.* Amsterdam: Elsevier Science Publishers B. V., 1989.
42. Johnson KL. *Contact Mechanics.* Cambridge: Cambridge University Press, 1994.
43. Wei Hsuin Y. The contact problem for viscoelastic bodies. *ASME.* 1966;33:395–401.
44. Berbner S, Loffler F. Influence of high temperatures on particle adhesion. *Powder Technol.* 1994;78(3):273–280.

45. German RG. *Sintering Theory and Practice*. New York: Wiley, 1996.
46. Pan J. Modelling sintering at different length scales. *Int Mater Rev*. 2003;48(2):69–85.
47. Haider C, Althaus T, Niederreiter G, Hounslow MJ, Palzer S, Salman AD. A micromanipulation particle tester for agglomeration contact mechanism studies in a controlled environment. *Meas Sci Technol*. 2012;23(10):105904.
48. Descamps N. *Glass Transition Effects on Mechanical and Surface Properties of Food Particles*. Ph.D. Thesis. Cork: Department of Process and Chemical Engineering, University College Cork, 2009.
49. Loret C, Meunier V, Frith WJ, Fryer PJ. Rheological characterisation of the gelation behaviour of maltodextrin aqueous solutions. *Carbohydr Polym*. 2004;57(2):153–163.